Comparative Effect of Rapid Dendrite Growth and Element Addition on Microhardness Enhancement of Fe-Based Alloys

Ying Ruan,*[,†,‡] Shou-Yi Chang,[§] and Ming Dao*[,‡]

†MOE Key Laboratory of Space Applied Physics and Chemistry, Department of Applied Physics, Northwestern Polytechnical University, Xi'an 710072, PR China

‡Department of Materials Science and Engineering, Massachusetts Institute of Technology, Cambridge, Massachusetts 02139, United States

§Department of Materials Science and Engineering, National Tsing Hua University, Hsinchu, 30013, Taiwan
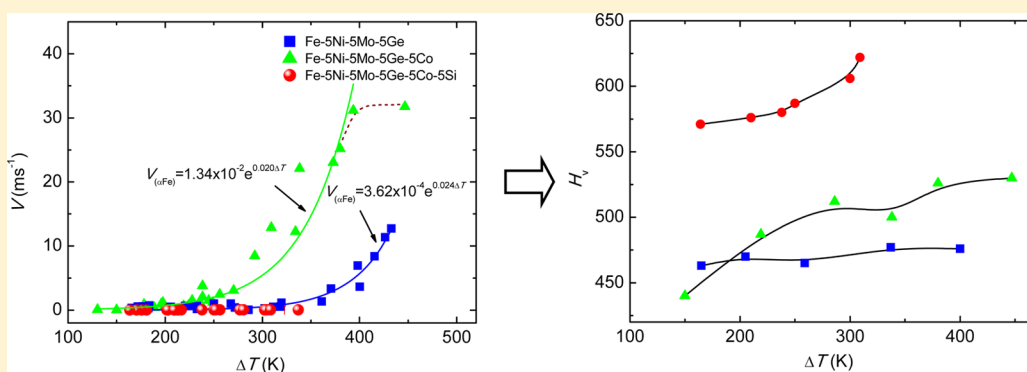
ABSTRACT: Herein, we adopted alloying and rapid-dendrite-growth methods to improve the mechanical properties of Fe-based alloys. Three molten alloys including Fe-5Ni-5Mo-5Ge, Fe-5Ni-5Mo-5Ge-5Co, and Fe-5Ni-5Mo-5Ge-5Co-5Si were undercooled, during which (αFe) dendrites grew rapidly with the decrease of temperature (i.e., increase of undercooling). The rapid growth of (αFe) dendrites in the Fe-5Ni-5Mo-5Ge-5Co alloy at a high rate of 31.8 ms^{-1} caused by a large undercooling more effectively enhanced the microhardness than a Co addition did. In comparison, because of the great disparity of atom size and valence electron number between Fe and Si, a further Si addition suppressed the (αFe) dendrite growth while dramatically increasing the Vickers microhardness of the Fe-5Ni-5Mo-5Ge-5Co-5Si alloy to H_V 622.

Fe-based alloys are attractive for a wide spectrum of engineering fields, since not only are they low cost but they also have excellent while tunable mechanical properties.[1−6] The mechanical properties of Fe-based alloys are important in practical applications and significantly influenced by solidification dynamics.[7−9] As a main solidification behavior, the dendrite growth of Fe can be realized by means of various methods, i.e., undercooling techniques, growth from solution or gas phases techniques, epitaxial growth techniques, and so forth.[10−13] For some single- or dual-phase Fe-based alloys, under undercooling condition, (αFe) solid solution in the form of dendrite rapidly grows and even transforms into fine equiaxial grain. Although the effect of dendrite/grain size on their mechanical properties was reported to follow the Hall-Petch relationship,[14−17] the correlation to the dynamic behavior of (αFe) dendrite growth has not yet been systematically characterized.

Besides rapid dendrite growth, the addition of alloying elements is another way to improve the mechanical properties of Fe-based alloys,[18,19] because the solubility of (αFe) phase can change, and a phase transition may occur during solidification. The effect of element additions (such as Co and Si) under the same undercooling condition on the mechanical properties of Fe-based alloys however remains unclear. Therefore, in this study, to comparatively study the influences of both a rapid dendrite growth and solute elements on the mechanical properties of Fe-based alloys, a series of multicomponent dual-phase (an (αFe) solid-solution phase and a dispersed Fe_7Mo_3 second phase) alloys including Fe-5Ni-5Mo-5Ge, Fe-5Ni-5Mo-5Ge-5Co, and Fe-5Ni-5Mo-5Ge-5Co-5Si alloys were prepared. The rapid solidifications of the undercooled molten alloys were accomplished using a sort of undercooling technique (named glass fluxing method) first, and the correlation among microhardness, dendrite growth rate, and alloying elements at different undercoolings were examined.

Three Fe-based alloys (compositions in wt %) were studied: Alloy 1 (Fe-5Ni-5Mo-5Ge), Alloy 2 (Fe-5Ni-5Mo-5Ge-5Co), and Alloy 3 (Fe-5Ni-5Mo-5Ge-5Co-5Si). Master alloy samples of 1 g were first prepared in an arc melting furnace with high-

purity Fe (99.99%), Ni (99.999%), Mo (99.99%), Ge (99.999%), Co (99.99%), and Si (99.999%). Cyclic super-heating of the alloys that were placed in a pure Al_2O_3 crucible and covered with a suitable amount of designed denucleating agent was then performed by a glass fluxing method in an Ar atmosphere (process chamber evacuated to a pressure of 2×10^{-4} Pa and refilled with ultrapure Ar to 10^5 Pa). Superheating by RF induction to temperatures of 100−300 K above the liquid temperature of the alloys and cooling at a relatively low rate were repeated several times to achieve a desired undercooling (denoted as ΔT). Subsequently, rapid solid-ification of the undercooled molten alloys was achieved by adjusting or switching off the heating power. The sample temperature was continuously monitored by a Yunnan-Land NQO8/15C infrared pyrometer, and the dendrite growth velocity was measured by an infrared photoelectric detector. The liquid temperatures, phase constitutions, and micro-structures of the samples were analyzed by a differential scanning calorimeter (DSC, Netzsch DSC 404C), an X-ray diffractometer (XRD, Rigaku D/max 2500 V), and a scanning electron microscope (SEM, FEI Sirion 200) with energy dispersive spectrometry (EDS, Oxford INCA 300). The microhardness of the alloys was measured by using a LECO LM248AT microhardness tester at an applied load of 500 gf and a dwell time of 15 s.

Figure 1 shows the SEM images and XRD patterns of Alloy 3 with different undercooling ranges; basically, Alloy 3 with a Si addition has the same phase constitution as those of Alloy 1 and Alloy 2.[20,21] During the rapid solidifications of all three undercooled Fe-based alloys, primary (αFe) dendrites first grew to form a main structure, between which a small amount of Fe_7Mo_3 as a second phase was dispersed in the interdendrite region. No (γFe) phase[22] was formed, as determined from the XRD analyses. As undercooling increased from 163 to 323 K, the (αFe) primary phase was observed to transform from dendrites with long arms into refined equiaxed grains. The main microstructure difference between Alloy 3 with a Si addition and the other two alloys was the appearances of a core Si-rich gray region and a surrounding Si-depleted dark region in the (αFe) dendrites, as determined by EDS analyses. Some of the Si solute atoms in Alloy 3 were expected to be expelled from the primary (αFe) dendrites during solidification, forming the surrounding (αFe) region with much less Si content.

Different undercooling ranges and solute elements change microstructures and in consequence yield very different mechanical properties, as shown by the measured Vickers microhardness (H_V) of the three Fe-based alloys in Figure 2. While the microhardness of Alloy 1 just slightly varied from H_V 463 to 476 with a markedly increased undercooling, the microhardness of Alloy 2 significantly increased from H_V 440 at a undercooling of 150 K to H_V 530 at a undercooling of 450 K.[21] Comparatively, for Alloy 3 in smaller undercooling ranges but with a Si addition, a significant increase in microhardness from H_V 571 to 622 was measured.

The crystal growth kinetics and energetics are determined by the initial material structure, as confirmed in the case of the epitaxial growth of $FeSi_2$ on Si substrates.[23−26] At low undercooling ranges, all three Fe-based alloys were believed to possess a similar microstructure and phases (mainly primary (αFe) dendrites and minor Fe_7Mo_3 dispersions) of similar sizes because of the same low level of dendrite growth rate ($V_{(\alpha Fe)}$, experimentally measured) as presented in Figure 3a. Accord-ingly, comparing Alloy 1 with Alloy 2, the same level of
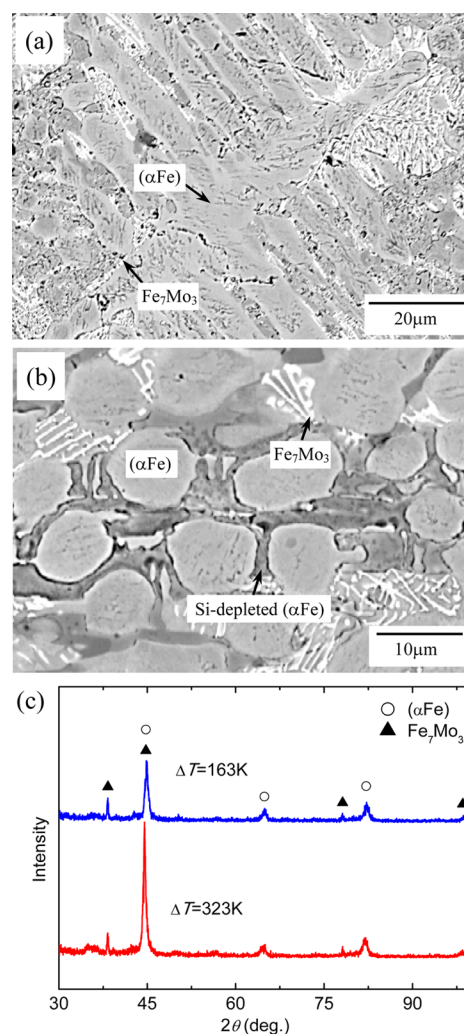
Figure 1. SEM microstructures of Alloy 3 with different undercooling ranges: (a) 163 K and (b) 323 K (gray phase: Si-rich (αFe), dark phase: Si-depleted (αFe), white phase: Fe_7Mo_3); (c) XRD patterns of undercooled Alloy 3.
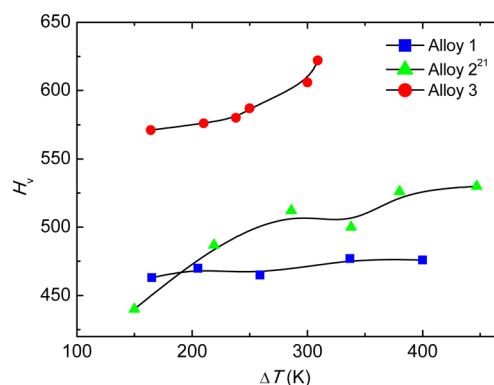
Figure 2. Microhardness of Fe-based alloys with different under-cooling ranges.

microhardness as low as about H_V 450 revealed the ineffectiveness of Co addition in terms of alloy solution strengthening due to the similar atom size and valence structure of Co to other alloy elements such as Fe and Ni. By contrast, solidification dynamics was found to be more crucial. With an enlarged undercooling range, the growth rate of (αFe)
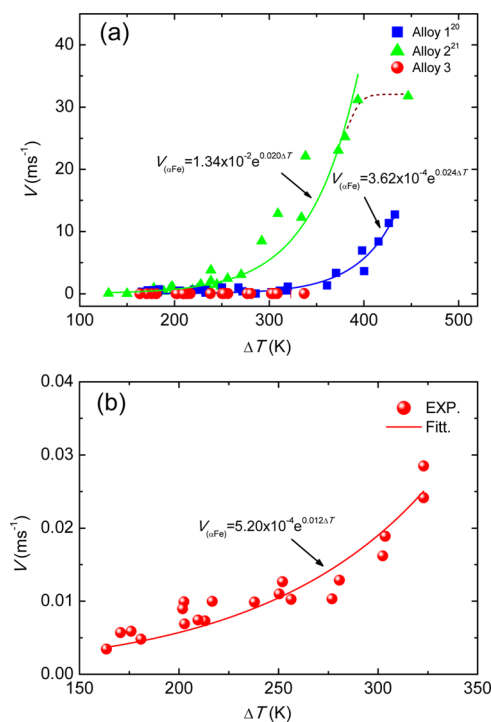
Figure 3. (a) Dendrite growth rates of Fe-based alloys with different undercooling ranges, (b) dendrite growth rate of Alloy 3.

dendrites increased to 12.7 ms^{-1} for Alloy 1 and to a much higher rate of 31.8 ms^{-1} for Alloy 2. Both dendrite growth rates followed an exponential relationship $V = A\exp(B\Delta T)$ with constants A and B (A: a function of solute concentration and diffusion; B: a function of dendrite formation heat),[20,27] although the dendrite growth of Alloy 2 slowed down at the late stage (marked by dashed line in Figure 3a) due to a saturated solidification fraction. For both alloys, B was determined to be around 0.022, indicating a similar dendrite formation heat despite the Co addition, while for Alloy 2, A was nearly 2 orders of magnitude larger than that of Alloy 1, revealing that a higher solute concentration contributed a faster dendrite growth. Especially for Alloy 2 with a Co addition, more solute accumulations around the solidified dendrites was expected to provide an additional constitutional undercooling that would greatly accelerate the growth of dendrites.[27,28] The increase in growth rate apparently refined the dendrite structure and consequently yielded the increased microhardness of Alloy 2.

At the same undercooling ranges, the growth rate of (αFe) dendrites in Alloy 3 with a Si addition was however highly suppressed to only 0.003 to 0.03 ms^{-1}, about 3 orders of magnitude lower than those found in Alloy 1 and Alloy 2 at its maximum achievable undercooling, as clearly shown in Figure 3b. Though the growth rate still followed the exponential relationship $V = A\exp(B\Delta T)$, the constant B for Alloy 3, 0.012, was only half of those of Alloy 1 and Alloy 2 (0.020 and 0.024). This implied a lower dendrite formation heat leading to a smaller driving force for solidification and consequently a slower growth rate of (αFe) dendrites in Alloy 3. Among these elements, it is well-known that the dendrite growth rate of pure Fe or Co, V_{Fe} or V_{Co}, is evidently larger than that of semiconductor Si, V_{Si}, at the same undercooling level. For example, as undercooling was 100 K, V_{Fe} and V_{Co} was measured to be 3 ms^{-1} and 9 ms^{-1} respectively,[29,30] which were two and

six times the value of V_{Si}, 1.5 ms^{-1}.[31] This is caused by the faceted growth and the large fusion enthalpy of Si. In the case of Fe-based alloy, the apparent lower dendrite formation heat (represented by B in $V = A\exp(B\Delta T)$) was caused by the semiconductor element Si. On one hand, the addition of Si lowered both interface kinetics and constitutional undercooling, according to LKT/BCT model.[20,32] On the other hand, the prior formation of the surrounding Si-depleted (αFe) region in Alloy 3 required additional time for more solute diffusion to proceed and to form a dendrite structure. Similarly, a relatively higher growth rate of dendrites at a larger undercooling range increased the microhardness of Alloys 3 owing to a refined microstructure as seen in Figure 1.

Compared with the case of very fast dendrite growth in Alloy 2, the solution hardening due to Si addition in Alloy 3 was found to be more effective than that due to Co addition; the dominance of Si addition in the markedly improved microhardness of Fe-based alloys was apparent, as shown in Figure 2. Si element improves the hardness of alloys commonly in two ways: (i) precipitation hardening, in which Si precipitates in the manner of high-strength metallic silicide or Si phase; (ii) solid solution hardening, in which Si exists as a solute. As reported, the hardness of Ti-based alloys increased with the addition of Si content due to the formation of metallic silicides Ti_2Ni_2Si and Ti_5Si_3 which were also used as reinforcement material in Fe- and steel-based alloys.[33] In some aluminum alloys, Si particles in the form of primary Si and eutectic Si phases served as dislocation generation sites. As Si content increased, the more refined dispersed Si particles and grain refinement by the increased Si particles resulted in the high increment of hardness.[34] For solid-solution hardening, it was reported that a Si addition raised the strain hardening of Fe-18Mn-0.6C TWIP steel and caused a significant improvement in yield strength of Fe-16Cr-25Ni stainless steel than an Al addition did.[22] Comparatively, the precipitated Si has greater contribution to the alloy's microhardness than the solid-solved Si in the same level.[35] In our experiments, neither metallic silicide nor Si phase was found in the Alloy 3, therefore Si remained in the (αFe) solid solution. The dissolution of alloying elements distorted αFe lattice. The lattice distortion yielded a sort of stress field interacting with dislocations and impeding their movement, consequently increasing the microhardness. Because of the differences in atom size and valence electron number between Fe and Si are larger than those between Fe and Co, more severe lattice distortions and strong covalent-like Fe−Si bonds in the Si-rich (αFe) dendrites and partly in the surrounding Si-depleted (αFe) region were believed to provide Alloy 3 a much higher solid-solution strengthening effect with the addition of Si.

In summary, the dependence of microhardness on (αFe) dendrite growth rates and solute elements Co and Si within Fe-based multicomponent alloys was systematically characterized. Compared with an Fe-5Ni-5Mo-5Ge alloy, the rapid growth of (αFe) dendrites in a 450 K undercooled Fe-5Ni-5Mo-5Ge-5Co alloy at a high rate of 31.8 ms^{-1} yielded a more significant hardening effect than a Co addition provided. A further Si addition suppressed the growth of (αFe) dendrites in an Fe-5Ni-5Mo-5Ge-5Co-5Si alloy to a rate below 0.03 ms^{-1}. However, a very strong solution-strengthening effect provided by Si addition enhanced the microhardness of the alloy markedly to a high level of H_V 622.

■ AUTHOR INFORMATION

Corresponding Authors
*E-mail: ruany@nwpu.edu.cn.
*E-mail: mingdao@mit.edu.

Notes
The authors declare no competing financial interest.

■ ACKNOWLEDGMENTS

■ REFERENCES

(1) Pasebani, S.; Charit, I.; Wu, Y. Q.; Butt, D. P.; Cole, J. I. *Acta Mater.* **2013**, *61*, 5605−5617.
(2) Liang, Y.; Liu, P.; Yang, G. W. *Cryst. Growth Des.* **2014**, *14*, 5847−5855.
(3) Ohmura, T.; Hara, T.; Tsuzaki, K. J.; et al. *J. Mater. Res.* **2004**, *19*, 79−84.
(4) Capdevila, C.; Miller, M. K.; Pimentel, G.; Chao, J. *Scr. Mater.* **2012**, *66*, 254−257.
(5) Torrens-Serra, J.; Stoica, M.; Bednarcik, J.; Eckert, J.; Kustov, S. *Appl. Phys. Lett.* **2013**, *102*, 041904−1−041904−4.
(6) Frontan, J.; Zhang, Y. M.; Dao, M.; Lu, J.; Galvez, F.; Jerusalem, A. *Acta Mater.* **2012**, *60*, 1353−1367.
(7) Singh, R.; Schneibel, J. H.; Divinski, S.; Wilde, G. F. *Acta Mater.* **2011**, *59*, 1346−1353.
(8) Fras, E.; Kawalec, M.; Lopez, H. F. *Mater. Sci. Eng., A* **2009**, *524*, 193−203.
(9) Woodcock, T. G.; Shuleshova, O.; Gehrmann, B.; Loser, W. *Metall. Mater. Trans. A* **2008**, *39*, 2906−2913.
(10) Gallego, J. M.; Miranda, R. *J. Appl. Phys.* **1991**, *69*, 1377−1383.
(11) Ouisse, T.; Sarigiannidou, E.; Chaix-Pluchery, O.; Roussel, H.; Doisneau, B.; Chaussende, D. *J. Cryst. Growth* **2013**, *384*, 88−95.
(12) Hamanaka, H.; Nakamura, Y.; Ishibe, T.; Kikkawa, J.; Sakai, A. *J. Appl. Phys.* **2013**, *114*, 114309−1−114309−5.
(13) Castle, E. G.; Mullis, A. M.; Cochrane, R. F. *J. Alloys Compd.* **2014**, *615*, S612−S615.
(14) Murakami, T.; Sahara, R.; Harako, D.; Akiba, M.; Narushima, T.; Ouchi, C. *Mater. Trans.* **2008**, *49*, 538−547.
(15) Mallikarjuna, C.; Shashidhara, S. M.; Mallik, U. S. *Mater. Des.* **2009**, *30*, 1638−1642.
(16) Attallah, M. M.; Davis, C. L.; Strangwood, M. *J. Mater. Sci.* **2007**, *42*, 7299−7306.
(17) Sangwal, K.; Surowska, B.; Blaziak, P. *Mater. Chem. Phys.* **2003**, *80*, 428−437.
(18) Jiao, Z. B.; Luan, J. H.; Zhang, Z. W.; Miller, M. K.; Ma, W. B.; Liu, C. T. *Acta Mater.* **2013**, *61*, 5996−6005.
(19) Rafiei, M.; Enayati, M. H.; Karimzadeh, F. *J. Mater. Sci.* **2010**, *45*, 4058−4062.
(20) Ruan, Y.; Dai, F. P. *Intermetallics* **2012**, *25*, 80−85.
(21) Ruan, Y.; Mohajerani, A.; Dao, M. manuscript in preparation, 2015.
(22) Jeong, K.; Jin, J. E.; Jung, Y. S.; Kang, S.; Lee, Y. K. *Acta Mater.* **2013**, *61*, 3399−3410.
(23) Derrien, J.; Chevrier, J.; Le Thanh, V.; Mahan, J. E. *Appl. Surf. Sci.* **1992**, *56*, 382−393.
(24) Yoshitake, T.; Nagamoto, T.; Nagayama, K. *Thin Solid Films* **2001**, *381*, 236−243.
(25) Nakamura, Y.; Nagadomi, Y.; Cho, S. P.; Tanaka, N.; Ichikawa, M. *Phys. Rev. B: Condens. Matter Mater. Phys.* **2005**, *72*, 075404−1−075404−7.
(26) Nakamura, Y.; Amari, S.; Naruse, N.; Mera, Y.; Maeda, K.; Ichikawa, M. *Cryst. Growth Des.* **2008**, *8*, 3019−3023.
(27) Peteves, S. D.; Abbaschian, R. *Metall. Mater. Trans. A* **1991**, *22*, 1271−1286.
(28) Sobolev, S. L. *Acta Mater.* **2013**, *61*, 7881−7888.
(29) Schleip, E. Ph.D. thesis, Univ. of Bochum, 1990.
(30) Drewes, K.; Schaefers, K.; Rösner-Kuhn, M.; Frohberg, M. G. *Mater. Sci. Eng., A* **1998**, *241*, 99−103.
(31) Aoyama, T.; Kuribayashi, K. *Acta Mater.* **2000**, *48*, 3739−3744.
(32) Lipton, J.; Kurz, W.; Trivedi, R. *Acta Metall.* **1987**, *35*, 957−964.
(33) Fornell, J.; Van Steenberge, N.; Suriñach, S.; Baró, M. D.; Sort, J. *J. Alloys Compd.* **2012**, *536S*, S186−S189.
(34) Cho, K. T.; Yoo, S.; Lim, K. M.; Kim, H. S.; Lee, W. B. *J. Alloys Compd.* **2011**, *509S*, S265−S270.
(35) Yang, Y.; Li, Y. G.; Wu, W. Y.; Zhao, D. G.; Liu, X. F. *Mater. Sci. Eng., A* **2011**, *528*, 5723−5728.